Check for updates

AGU ADVANCING EARTH AND SPACE SCIENCE

Water Resources Research

RESEARCH ARTICLE
10.1029/2020WR027463

Permafrost Promotes Shallow Groundwater Flow and Warmer Headwater Streams

Ylva Sjöberg[1], Ahmad Jan[2], Scott L. Painter[2], Ethan T. Coon[2], Michael P. Carey[3], Jonathan A. O'Donnell[4], and Joshua C. Koch[3]

[1]Department of Geosciences and Natural Resource Management, CENPERM Center for Permafrost, University of Copenhagen, Copenhagen, Denmark, [2]Climate Change Science Institute & Environmental Sciences Division, Oak Ridge National Laboratory, Oak Ridge, TN, USA, [3]U.S. Geological Survey, Alaska Science Center, Anchorage, AK, USA, [4]National Park Service, Arctic Network, Anchorage, AK, USA

Key Points:

- Models of hillslope permafrost show that groundwater flow paths deepen as permafrost thickness and extent decreases
- Less permafrost, and therefore deeper flow paths, result in reduced evapotranspiration and increased groundwater discharge
- Model and observations show that shallow permafrost leads to higher July stream temperatures, suggesting streams will cool as soils warm

Supporting Information:

- Supporting Information S1

Correspondence to:
Y. Sjöberg,
ys@ign.ku.dk

Citation:
Sjöberg, Y., Jan, A., Painter, S. L., Coon, E. T., Carey, M. P., O'Donnell, J. A., & Koch, J. C. (2021). Permafrost promotes shallow groundwater flow and warmer headwater streams. *Water Resources Research*, *57*, e2020WR027463. https://doi.org/10.1029/2020WR027463

Received 13 MAR 2020
Accepted 4 DEC 2020

Abstract The presence of permafrost influences the flow paths of water through Arctic landscapes and thereby has the potential to impact stream discharge and thermal regimes. Observations from 11 headwater streams in Alaska showed that July water temperatures were higher in catchments with more near-surface permafrost. We apply a fully coupled cryohydrology model to investigate if the impact of permafrost on flow path depth could cause the same pattern in temperatures of groundwater discharging from hillslopes to streams. The model simulates surface energy and water balances, snow, and subsurface water and energy balances for two-dimensional hillslope model cases with varying permafrost extent. We find that hillslopes with continuous permafrost have more shallow flow paths and twice as high rates of evapotranspiration, compared to hillslopes with no permafrost. For our simulated cases, 6.7% of the horizontal water flux moves through the top organic soil layers when there is continuous permafrost, while only 0.5% moves through organic layers without permafrost. The deeper flow paths in permafrost-free simulations buffer seasonal temperature extremes, so that summer groundwater discharge temperatures are highest with continuous permafrost. Our results suggest that permafrost thawing alters groundwater flow paths and can lead to decreases in summer stream temperatures and reductions in evapotranspiration in headwater catchments. These changes are of potential importance for stream biotic components of ecosystems, however, the full impact remains unknown.

1. Introduction

Permafrost exerts a primary control on the hydrology of Arctic regions by impeding infiltration and flow through the ground. Following the rapid air temperature increases projected for the Arctic, widespread thaw of near-surface (top 2 m) permafrost is expected within this century, extending into the continuous permafrost zone (ACIA, 2004; Chadburn et al., 2017; Hansen et al., 1999; Koven et al., 2013; Turner et al., 2007). Hydrological shifts associated with permafrost thaw constitute a critical uncertainty when projecting fluxes of water, energy, sediments, and solutes to fluvial and marine ecosystems (Bring et al., 2016; Hinzman et al., 2005). The transfer of carbon and nutrients via groundwater in permafrost terrain to surface waters will likely alter aquatic ecosystem productivity, driving bottom-up shifts in food web dynamics (Creed et al., 2018; Kendrick et al., 2018). Changes in groundwater discharge associated with permafrost thaw may also alter the thermal regime of surface waters, which functions as a primary control on ecosystem and organismal processes.

Recent observation- and modeling-based studies have provided insight into the mode of hydrological changes expected with thawing permafrost. Groundwater flow paths are generally shallow and rapid in watersheds or hillslopes underlain by permafrost (Koch, Ewing, et al., 2013; Koch, Runkel, et al., 2013; O'Connor et al., 2019), partially because subsurface ice can create an impermeable boundary that limits longer, deeper flow. With active layer thickening or wholesale loss of permafrost, groundwater flow paths are expected to deepen and groundwater transit times increase (Frampton & Destouni, 2015; Walvoord et al., 2012). With deeper and longer flow paths, groundwater discharge areas are expected to move downslope toward the lowlands in river basins, which could result in drier conditions for today's low-order streams (Lamontagne-Hallé et al., 2018; Walvoord et al., 2012). Interacting with flow path depth, evapotranspiration controls the amount of water available for runoff at catchment scales. Expected increases in air

© 2020. The Authors.
This is an open access article under the terms of the Creative Commons Attribution-NonCommercial-NoDerivs License, which permits use and distribution in any medium, provided the original work is properly cited, the use is non-commercial and no modifications or adaptations are made.

temperature and precipitation (Bintanja & Selten, 2014), may lead to higher evapotranspiration rates, but deeper flow paths and lower near-surface soil moisture could counteract such processes and instead lower actual evapotranspiration rates. For regional scale projections, earth system models provide a wide range of responses in hydrology to changes in permafrost, and while decreasing soil moisture is projected by most models, changes in runoff-evapotranspiration ratios are inconsistent across models (Andresen et al., 2020; Koven et al., 2013).

A warming Arctic climate is expected to also alter the thermal regime of streams. Lammers et al. (2007) analyzed observed temperatures for Arctic rivers in Russia for the 1929–2003 period and found that river temperatures and energy fluxes had not increased in concert with regional air temperatures. They speculated that possible reasons for this offset could be either increasing impacts of human impoundments, increasing inputs from melting ground ice, increased evaporation from river surfaces, or deepening of flow paths following permafrost thaw. The thermal impact from evaporation and human impoundments on river temperatures in permafrost areas have been the focus of a few studies (Cozetto et al., 2006; Fabris et al., 2020; King et al., 2016; Yang et al., 2005). However, to our knowledge, no attempt to quantify the potential influence of changes in flow paths has been made to follow up on these suggested mechanisms in Arctic river basins.

The temperature of stream water is a function of the temperature of source waters that enter the stream and in-stream processes, such as heating from incoming shortwave and longwave radiation. Groundwater discharge and snowmelt are often considered as buffers for air temperature increases, at least for short time-scales, as they provide relatively cold water (Leach & Moore, 2019; Lisi et al., 2015). First-order streams receive most of their water from groundwater and a general warming trend is usually seen with increasing stream order as water warms within streams (Caissie, 2006; Fabris et al., 2020; Kelleher et al., 2012; Zwieniecki & Newton, 1999). The thermal dynamics of discharging groundwater is controlled by the ground thermal regime and the depths of groundwater flow paths, and changes in either of these factors with permafrost thaw could therefore theoretically influence temperatures in first-order streams and subsequently affect higher order stream systems.

Hydrological models with freeze-thaw representation (cryohydrology models) can be used to identify flow paths and quantify groundwater discharge and recharge rates related to dynamic permafrost and seasonal soil freezing (Bense et al., 2012; Frampton et al., 2013; Kurylyk et al., 2016; McKenzie & Voss, 2013). Such models offer capabilities to isolate effects of changes in single ecosystem components such as permafrost, which are in field observations often masked by complexly interacting processes in Arctic catchments. Recent developments in cryohydrology modeling includes coupling of snow, surface energy balance, and surface flow, with variably saturated cryogeohydrology (Endrizzi et al., 2014; Jan et al., 2018; Painter et al., 2016) and have provided insights into permafrost hydrology across a range of terrain types (Abolt et al., 2018; Atchley et al., 2016; Harp et al., 2016; Jafarov et al., 2018; Sjöberg et al., 2016). Even though field observations have informed the setup of many of these modeling studies, simulation results (e.g., subsurface temperature and groundwater discharge) are rarely directly related to catchment-scale empirical data (e.g., stream discharge, temperature, and chemistry). Instead, these model studies provide a complementary understanding of ecosystem processes which can guide interpretations of observations from Arctic catchments.

In this study, we identify a pattern of increasing summer stream temperatures with permafrost extent for 11 headwater streams in northwestern Alaska (Section 2) and apply a generic cryohydrology model to test if permafrost-induced flow path differences can yield temperature differences of groundwater discharge that could explain the observed pattern (Section 3). Our model simulates saturated, unsaturated, and surface flow and energy, and snow processes, for hillslope cases with various permafrost extent. From the simulation results, we quantify the effects of permafrost distributions on hillslope hydrology with regards to: (i) partitioning of precipitation between evapotranspiration, overland and subsurface runoff and storage, (ii) the depth of flow paths, and (iii) groundwater discharge temperatures (Section 4). We discuss how to interpret these results in light of ongoing Arctic warming and permafrost loss, focusing on runoff magnitude, timing, and temperature because these are variables that govern stream biogeochemical cycling, ecosystem processes, and fish presence, growth, and reproduction (Section 5). The results provide a mechanistic basis for interpreting field observations from streams in terms of permafrost characteristics and thaw.

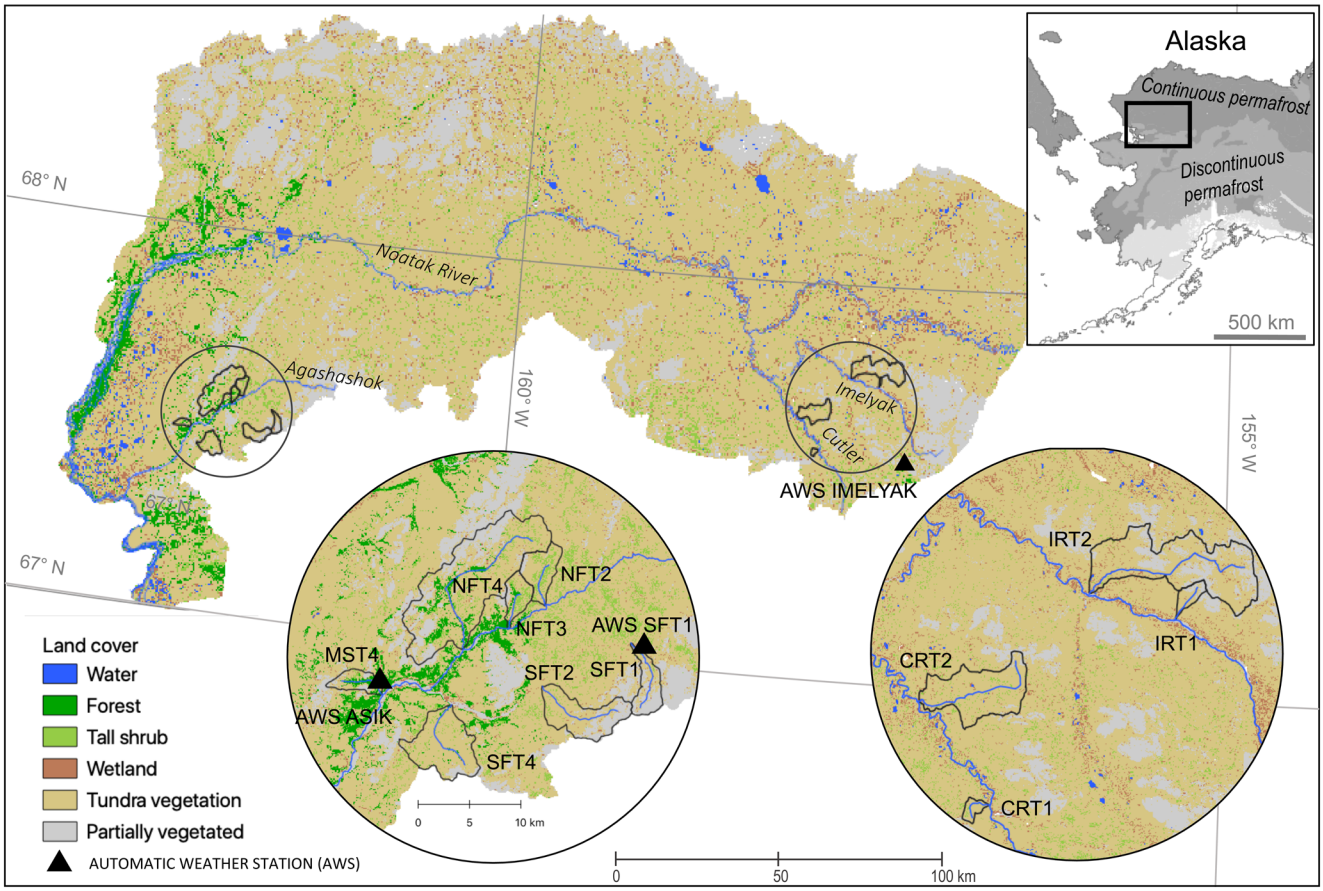


Figure 1. Location of the sites in the Noatak National Preserve, where field data were collected. Catchments outlines for streams where samples and observations were collected in the Agashashok, and Cutler and Imelyak River basins are shown in black. NFT4 is a fourth order stream, SFT4 is a second order stream, and all other streams are of the first order. (Land cover data modified from Jorgensen et al. (2009), permafrost data from Brown et al. (2002).

2. Streams in the Noatak National Preserve

2.1. Physical Setting

We have studied headwater stream catchments in the Agashashok, Cutler, and Imelyak River basins located in the Noatak National Preserve in northwestern Alaska, near the boundary between the discontinuous and continuous permafrost zones (Figure 1) (Brown et al., 2002). The Noatak National Preserve is located in the boreal-arctic transitional area where Arctic tundra and boreal spruce forests are the dominant vegetation types. Surficial geology is characterized by bedrock and poorly developed soils in the Agashashok area and by glaciolacustrine sediments in the Cutler-Imelyak area (Hamilton, 2010; O'Donnell et al., 2016). The slopes along the observed streams in the Cutler-Imelyak sites are covered by ice-wedge polygons, which indicates the presence of relatively ice-rich permafrost. Along the Agashashok streams, the slopes near the observation points are free of landforms that suggest ice-rich permafrost, and soil pits, continuous loggers, and geophysical surveys (M. Briggs and J. Koch, U.S. Geological Survey, written communication) suggest that thaw is on the order of decimeters to meters in the summer. Tundra is the dominating vegetation type along streams in the Cutler-Imelyak catchments, while forest cover is commonly found along the streams in the Agashashok catchments, although tundra vegetation dominates at the catchment scale. An extensive mapping of ecotypes, with associated soil and permafrost characterization, has been undertaken by Jorgenson et al. (2009) for the region covering all of our studied headwater catchment sites. The ecotype classification was based on 724 field plots where vegetation, soils, and permafrost were investigated, and upscaled using Landsat ETM + satellite imagery. The main ecotypes for our sites are alpine barren, upland shrub, and upland meadow ecotypes, except for in MST4 where forest covers >20% of the catchment. We

used the permafrost characteristics associated with the ecotypes to quantify the fraction of the near-stream (<1,000 m from stream) catchment area that is underlain by near-surface (<1 m from surface) permafrost (Table 1).

2.2. Summer Stream Temperatures

Stream temperatures were observed at 15-min intervals at 62 locations in nine first-order, one second order, and one fourth order streams in the Agashashok, Cutler, and Imelyak river basins for the summer of 2017 (Figure 1, Carey et al., 2020). The streams ranged in width from 5 to 28 m and in mean depth from 0.1 to 0.36 m near the outlets. Temperature data were collected at 15-min intervals using Onset (Bourne, MA) Tidbit V2 temperature sensors (±0.21°C) and In Situ (Fort Collins, CO) pressure transducers (Rugged Troll 100s [accuracy ±0.3°C] and Level Troll 500s and 700s [accuracy ±0.1°C]). In the catchments, one pressure transducer was placed near the outlet of the tributary, one Tidbit sensor was placed in a pool upstream of the pressure transducer, and another Tidbit in a run with minimal mixing. Upstream of the outlet, approximately 250–1,000 m depending on constraints of helicopter access, Tidbit sensors were also placed in pool and run locations. The Tidbit sensors were placed in contact with the stream bed, secured with a duck-billed anchor, and shaded from solar radiation by undercut banks or rocks. For some of the streams, extra sensors were deployed; not all sensors could be retrieved at the end of the season (see Table S1 for stream sensors details). Quality assurance and control followed procedures outlined in Sowder and Steel (2012) and included checks for de-watering events and sensor calibration (M. P. Carey et al., 2020). The 51 sensors that remained after retrieval and quality check were used in the following analyses (Table S1).

The temperature of groundwater discharging to streams is expected to be most sensitive to groundwater flow path depth during July, as the thermal gradients with soil depth are strongest during the peak season for air temperature (Koch, O'Donnell, & Carey, 2020). Equally strong thermal gradients could be expected in soils during the winter but would impact stream temperatures less, as frozen soil conditions impede groundwater flow. July is also after the snowmelt period in the study area based on diel snow pulses observed in the discharge hydrographs (Koch et al., 2019), meaning that all the water in the streams can be assumed to originate from shallow runoff or groundwater discharge. The potential effect from in-stream thermal processes is limited by generally short (<1 day) transit times, as determined in three of the streams based on stream lengths, and tracer velocities calculated following methods in Runkel (2007).

Observed stream temperatures in July show strong positive regressions with increasing permafrost cover (Figure 2). The regression is strongest for daily median temperature ($R^2 = 0.78$, $p < 0.001$), slightly weaker for daily maximum temperature ($R^2 = 0.76$, $p < 0.001$), and weakest for minimum temperature ($R^2 = 0.64$, $p < 0.005$). Air temperatures were similar between the three weather stations, but slightly warmer for the stations near the Agashashok sites (SFT1: 14.0 ± 4.0°C, Asik: 12.8 ± 3.4°C) which exhibit colder stream temperatures on average than the Cutler-Imelyak sites, than for the Imelyak station (10.8 ± 3.1°C). This suggests that air temperature differences do not drive the observed differences in stream temperatures. Although there is some uncertainty associated with the estimates of permafrost cover along streams and variability in observed temperatures within streams, the observed pattern suggests that permafrost may exert a control on summer stream temperatures in our study area.

3. Model Experiment

3.1. Aims and Assumptions

We hypothesize that differences in flow path depths induced by permafrost extent can cause stream temperature patterns such as those observed in our Noatak streams. To test this hypothesis, we set up generic 2D model configurations for hillslope cases representing plausible current and future permafrost conditions for the region. We model three cases: (i) a permafrost-free case containing only seasonal frost, (ii) a discontinuous permafrost case containing a block of permafrost in the domain, and (iii) a continuous permafrost case containing permafrost in the whole domain except for the active (seasonally thawed) layer. The only differences in model configuration between these cases were the thermal boundary conditions at the bottom

Table 1
Catchment Area, Stream Length, and Near Surface Permafrost Cover Within 1,000 m From the Stream, and Percentage Cover of Ecotypes With Associated Depth to Permafrost Within 1,000 meters From the Stream in Each Catchment, From Jorgenson et al. (2009)

		MST4	NFT2	NFT3	NFT4	SFT1	SFT2	SFT4	IRT1	IRT2	CRT1	CRT2
Catchment area (km^2)		8.6	13.7	9.0	93.8	12.3	25.9	32.6	1.4	73.5	3.4	41.4
Stream length (km)		5.2	5.0	4.0	17.6	7.7	9.2	8.1	3.2	13.6	3.8	18.4
Near-surface permafrost (%)		25	47	42	39	28	52	72	55	63	72	67
Ecotype	N											
Permafrost within 1 m depth												
Lowland Sedge Fen	25	0.3	0.1	0.2	1.1	0.3	0.8	0.3	2.1	3.6	0.3	2.8
Lowland Ericaceous Shrub Bog	21	0.0	0.0	0.0	0.0	0.0	0.0	0.0	4.0	3.6	0.1	0.7
Lowland Birch-Ericaceous-Willow Low Shrub	11	0.4	0.4	0.6	0.7	0.2	0.8	0.9	1.6	4.0	3.2	5.1
Lowland Willow Low Shrub	7	0.0	0.2	0.0	0.0	0.0	0.1	0.0	1.5	1.8	0.5	0.8
Lowland Alder Tall Shrub	4	0.9	1.4	0.5	0.8	0.0	0.4	0.2	0.0	0.5	0.6	1.7
Upland Sedge-Dryas Meadow	9	9.1	2.2	3.8	8.8	12.2	11.1	5.4	29.7	22.8	6.7	9.9
Upland Willow Low Shrub	7	4.1	6.9	5.1	4.5	1.9	2.7	2.5	14.2	6.8	7.7	7.3
Upland Dwarf Birch-Tussock Shrub	38	10.1	34.9	26.4	35.3	16.0	41.4	69.6	12.8	20.9	48.0	43.5
Permafrost within 2 m depth												
Alpine Wet Sedge Meadow	4	1.4	0.3	0.6	0.9	1.7	1.1	0.2	0.2	0.6	0.3	0.1
Upland Birch-Ericaceous-Willow Low Shrub[a]	8	10.3	20.7	13.1	14.2	6.5	10.1	9.9	2.2	5.9	23.3	17.8
Permafrost below 1 m depth												
Alpine Alkaline Barrens[b]	1	9.5	0.0	0.0	4.7	51.1	25.1	3.7	23.9	20.2	3.3	3.9
Alpine Mafic Barrens[c]	0	4.8	0.0	0.0	0.0	0.0	0.0	0.0	0.0	0.0	0.0	0.0
Alpine Acidic Barrens[b]	2	2.0	0.3	10.5	0.5	0.5	0.1	0.0	0.0	0.1	0.0	0.0
Alpine Dryas Dwarf Shrub[b]	2	12.3	2.6	2.7	5.0	6.2	2.8	0.8	6.7	7.2	0.7	2.0
Alpine Ericaceous Dwarf Shrub	2	2.9	0.5	0.7	1.1	1.9	0.8	0.3	1.0	1.4	0.1	0.8
Permafrost below 1 m depth or absent												
Upland Alder-Willow Tall Shrub[d]	4	5.1	29.6	23.8	9.3	1.3	2.7	4.0	0.0	0.1	5.1	3.4
Upland White Spruce Forest[d]	2	23.3	0.0	11.2	10.9	0.0	0.0	1.7	0.0	0.0	0.0	0.0
Permafrost below 1.3 m depth or absent												
Upland White Spruce-Lichen Woodland[e]	0	0.6	0.0	0.3	1.0	0.0	0.0	0.3	0.0	0.0	0.0	0.0
Permafrost below 2 m depth or absent												
Upland Spruce-Birch Forest[f]	0	1.4	0.0	0.4	0.4	0.0	0.0	0.0	0.0	0.0	0.0	0.0
Upland Birch Forest[g]	0	1.6	0.0	0.2	0.7	0.0	0.0	0.1	0.0	0.0	0.0	0.0
Permafrost absent												
Lowland Lake[h]	0	0.0	0.0	0.0	0.0	0.0	0.0	0.0	0.0	0.3	0.0	0.4

Notes. Ecotype classes are grouped by the associated permafrost class used in Figure 2. N refers to the number of observations of thaw depth (frost table) in soil pits. Soil stratigraphy is in total described for 542 sites from soil pits or shallow soil cores, within the ecotypes occurring in our catchments.

[a]At some sites (additional to listed N) the frost table could not be observed, as commented by Jorgensen et al: "Thaw depths often could not be determined in the rocky soils, but permafrost is presumed to be present with in the upper 2 m of the soil profile." [b]At some sites (additional to listed N) the frost table could not be observed, as commented by Jorgensen et al: "Thaw depths often could not be determined in the rocky soils, but permafrost is presumed to be present below 1 m due to cold temperatures at the high elevations." [c]Comment by Jorgenson et al.: "permafrost is presumed to be present below 1 m due to the cold temperatures at the high elevations." [d]At some sites (additional to listed N) the frost table could not be observed, as commented by Jorgensen et al: "Thaw depths often could not be determined in the rocky soils, but permafrost is presumed to be absent or to occur below a depth of 1 m." [e]Comment by Jorgenson et al.": Thaw depths could not be determined as the depth to permafrost, if present, was always greater than the maximum depth sampled (1.3 m)." [f]Comment by Jorgenson et al.: "Thaw depths could not be determined in the rocky soils, but in most cases permafrost is presumed to be absent or to occur below a depth of 2 m." [g]Comment by Jorgenson et al.: "Thaw depths often could not be determined in the rocky soils, but permafrost is presumed to be absent or to occur below a depth of 2 m." [h]Comment by Jorgenson et al., 2009: "Flooded soils were not described."

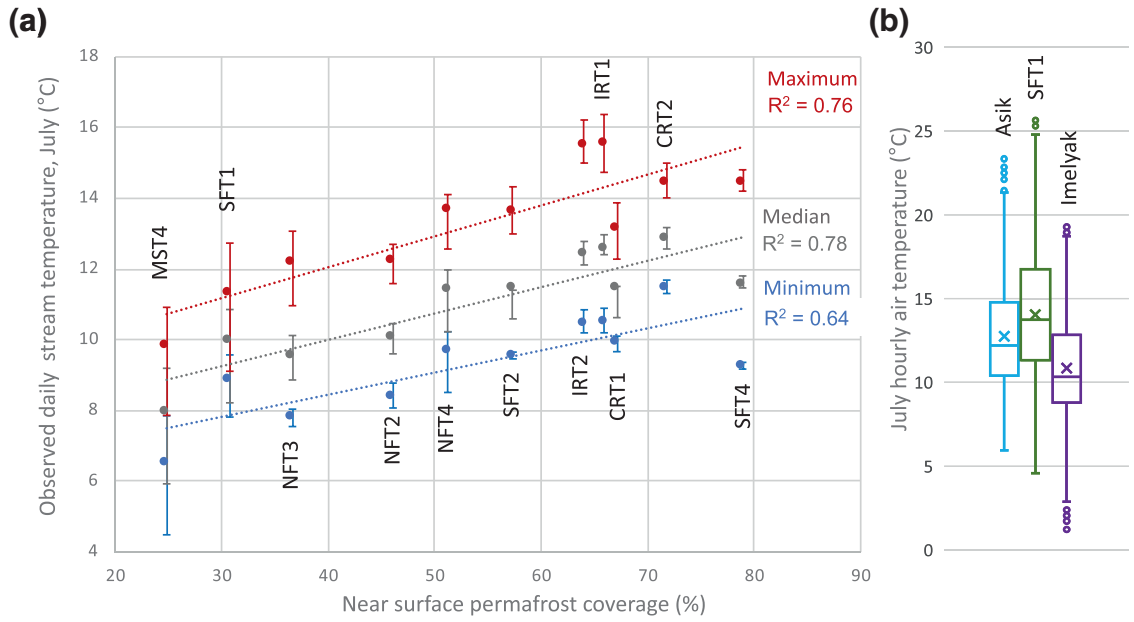


Figure 2. Regression plot of near surface permafrost coverage (from Table 1) and observed daily stream temperature in July 2017(a). Error bars show average values for the coldest and warmest sensor in each stream. Number of sensors deployed per stream is 5, except for in MST4 ($N = 6$), NFT4, CRT1, and CRT2 ($N = 4$), and SFT2 ($N = 3$). Hourly observed air temperatures for stations in Agashashok (Asik and SFT1) Cutler-Imelyak (Imelyak) areas, for July 2017 (b). Boxplots show interquartile ranges (box), median (line), mean (x), 5th and 95th percentile (error bars), and outliers (circles). Locations of named sites and weather stations can be found in Figure 1.

of the domain and the spatial distribution of snow (described below). Our model experiment is based on a set of assumptions, of which the most fundamental are that seasonal freezing/thawing will influence the permeability of the soil and the ground latent heat flux and that the unsaturated and saturated zones are dynamically evolving based on the climatic forcing in the model (i.e., a variable water table). The simplified 2D geometry makes it straight-forward to compare results between cases and relate them to flow path depths. However, the lack of (micro)topography precludes local groundwater circulation and water retention on the ground surface, which may limit infiltration and evapotranspiration rates compared to catchment-scale field observations. We further assume that evapotranspiration can be simulated with reasonable results by representing near-surface water availability only and excluding the transpiration of deeper water through deeper vascular plant roots (Jan et al., 2020). It is important to note that we do not assume that the temperature of groundwater discharge can fully explain observed stream temperature dynamics, as in-stream processes likely modify the water temperature.

3.2. Tool

The Advanced Terrestrial Simulator (ATS) version 0.88 (Coon et al., 2019) was chosen as the modeling tool due to its ability to realistically represent the full range of physical processes associated with the model assumptions, including surface and subsurface thermal (freeze-thaw) hydrology coupled with surface energy balance (Atchley et al., 2015; Painter et al., 2016). The ATS is an open-source parallel software tool for numerical simulation of a range of coupled physical processes related to flow and transport and includes several process models specific for cold region hydrology. ATS solves a modified Richards equation and an energy transport equation for variably saturated, variably frozen flow in permafrost-rich soils. This approach is based on the "freezing equals drying" approximation by which water phase change alters the capillary pressure through the Clapyron equation and in effect controls the hydraulic properties of the ground (Painter & Karra, 2014). This is coupled to a modified diffusion wave approximation and energy transport equations for flow on the soil surface, an energy balance equation which calculates evapotranspiration and snow thermal properties, and, for one set of simulations, a simple diffusion equation describing snow

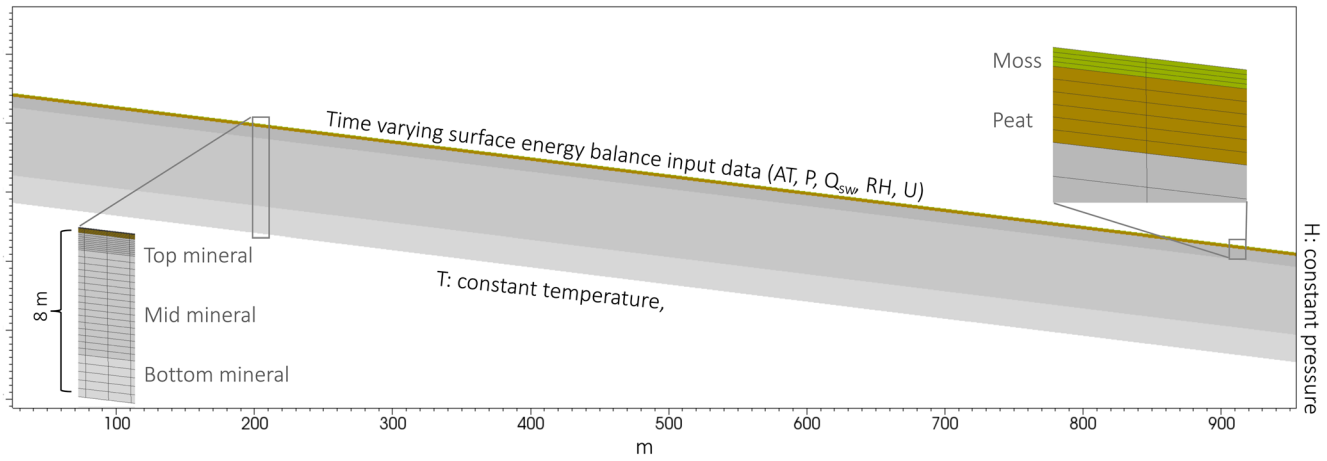


Figure 3. Geometry, specified thermal (T) and hydrological (H) boundary conditions, and soil layers represented in the modeling mesh. No specified thermal and hydrological conditions constitute no flow boundaries. The surface energy balance model is driven by daily data for air temperature (AT), snow and rain precipitation (P), shortwave radiation (Q_{sw}), relative humidity (RH), and wind speed (U). (Note that the geometry is modified to optimize visualization of soil layers, by exaggerating the thickness [8 m] while maintaining the slope [0.1] of the domain).

distribution. Loss of water from the land surface is calculated from explicit surface energy and water balances with ground heat flux coming from ATS, resulting in an estimate of potential evapotranspiration, as in the Penman-Monteith and Priestly-Taylor models. The potential evapotranspiration is then limited by soil water availability, based on liquid water content on the surface. This approach does not include an explicit partitioning between transpiration and evaporation and potentially underestimates evapotranspiration in the case where deep-rooted vascular plants access deeper water, but that is rarely the case in the study area, where plants have relatively shallow rooting depths (Canadell et al., 1996; Jorgenson et al., 2009). This model has previously been tested against observed eddy covariance evapotranspiration data for a tundra environment with reasonable results (Jan et al., 2020). ATS simulations were also evaluated against observations of soil temperature and water table depth at multiple locations across multiple years at the same site with very good results (Jan et al., 2020). Required inputs to simulate flow and energy in permafrost-rich soils include meteorological data, soil structure and parameterizations for porosity, permeability, water retention curves and thermal conductivities, and surface balance parameters such as albedo and desiccated thickness, along with thermal and hydrologic boundary conditions.

3.3. Domain

The model domain was 1,000 m in the horizontal (x) direction, 8 m thick (z), and had a slope of 0.1, which is representative of the slopes where our field observations were made. The cell size was 10 m in the x-direction. In the vertical direction, the cell size increased with depth following five layers representing, from the top, moss (live and dead), peat (decomposing moss, litter, and root layer), and three mineral-soil layers (Figure 3). Ground thermal and hydraulic properties, which are variable with temperature in ATS, were taken from either local samples or literature values for soils similar to those observed at our sites (Table 2). Local soil samples were taken from soil pits dug in the active layer (typically 0–50 cm below ground surface) at 11 locations near the streams in the Agashashok basins and in nine locations near the streams in the Cutler-Imelyak basins (Table 3) (Koch, Sjöberg, & Carey, 2020). Permeability (infiltration capacity) was measured in the field using a Guelph permeameter screened at different depths in the Agashashok soil pits. Soil samples were retrieved in 5.1 cm diameter PVC sleeves from four of the Agashashok soil pits and three of the Imelyak and Cutler soil pits. Samples were shipped to the Daniel B. Stephens and Associates, Inc. laboratory in Albuquerque, NM, for the following analyses: (i) constant and falling head tests for measuring hydraulic conductivity, which was later converted to permeability; (ii) hanging column and pressure plate, as well as dew point potentiometer and relative humidity box methods for measuring water retention characteristics; and (iii) measurements of thermal properties using a Decagon KD2 Pro probe.

Table 2
*Physical Properties Used in the Model**

	Moss	Peat	Top mineral[a]
Thickness [m]	0.05	0.2	7.75
Porosity [−]	0.95	0.88	0.6
Permeability [m^2]	5.e−11	1.5e−11	2.e−12
Van Genuchten alpha [Pa^{-1}]	2.35e−3	6.e−5	3.e−6
Van Genuchten m [−]	0.28	0.22	0.24
Van Genuchten residual saturation [−]	0.056	0.	0.05
Thermal conductivity, saturated [$Wm^{-1}K^{-1}$]	0.57	0.699	1.1
Thermal conductivity, dry [$Wm^{-1}K^{-1}$]	0.07	0.095	0.15

*For a full description of how physical properties change with temperature and phase in the model, see Painter et al. (2016).
[a]The model domain contained three mineral layers with the same physical properties as listed. The three layers differed in cell thickness, from 0.033 m (top mineral, 0.9 m thick), to 0.3 m (mid mineral, 4.85 m thick), to 0.4 m (bottom mineral, 2 m thick).

3.4. Boundary Conditions

All three permafrost cases had hydraulic no-flow boundaries at the bottom and left (top of slope) side of the domain, and a hydrostatic boundary with atmospheric pressure at the ground surface at the right-side boundary. The continuous permafrost case had a thermal boundary at the bottom side of the domain of −2.5°C, while the discontinuous permafrost and permafrost-free cases had a bottom boundary temperature of 1°C. Simulations with a deeper mesh (50 m) indicate that the seasonal temperature variation at the

Table 3
Tested Hydraulic and Thermal Properties of Soils in the Study Area (Marked With x)

Sub-catchment	Soil description	Depth [m]	Porosity	Van G. α[a]	Van G. N[b]	Res. Sat.[c]	K[d]	K[e]	K[f] Guelph
MST4/Asik	Fine-grained mineral	0.20–0.27	x	x	x	x	v		
MST4	Fine-grained mineral	0.13							x
MST4	Coarse-grained mineral	0.39							x
SFT1	Fine-grained mineral with cobbles	0.38							x
SFT1	Coarse-grained mineral	0.25							x
SFT1	Organic	0.0–0.7	x	x	x	x	h	x	
SFT1	Organic	0.0–0.7	x	x	x	x	h		
NFT3	Fine-grained mineral	0.17							x
NFT3	Fine-grained mineral with cobbels and rocks	0.18							x
NFT3	Fine-grained mineral	0.1–0.17	x	x	x	x	h		
NFT3	Fine-grained mineral	0.18							x
NFT3	Coarse-graine mineral	0.35							x
NFT3	Fine-grained mineral	0.27							x
NFT3	Fine-grained mineral	0.23							x
IRT1	fine-grained mineral with cobbles	0.3–0.37	x	x	x	x	v		
CRT2	Fine-grained mineral	0.12–0.19	x	x	x	x	v		
CRT1	Fine-grained mineral	0.14–0.30	x	x	x	x	v	x	

[a]Van Genuchten alpha parameter. [b]Van Genuchten N parameter. [c]Residual saturation. [d]Permeability, tested in laboratory. Denoted v for vertical samples, and h for horizontal samples. [e]Thermal conductivity. [f]Permeability measured in the field with Guelph permeameter.

bottom boundary of our configurations is <0.1°C, which motivates using a computationally simplifying steady temperature bottom boundary condition for our simulations. The left and right boundaries had no specified thermal conditions. With these boundary conditions, permafrost conditions were at steady-state after spin-up (described below), over the time-scales of our simulations.

3.5. Top Boundary—Weather Data

Locally observed air temperature, precipitation, relative humidity, wind speed, and modeled incoming shortwave radiation defined the time-varying (daily) boundary conditions for the surface energy balance model at the domain surface. Data from the National Park Service's Asik weather station from late 2012 until late 2016 were combined with data from the U.S. Geological Survey's SFT1 station from late 2015 to late 2017 (see Figure 1, for station locations) (Hill & Sousanes, 2018; Koch, Carey, et al., 2020). A 1-year time series of air temperature data was generated by calculating mean daily air temperature for each day of year over this period. For rain/snow (defined as observed precipitation for days when air temperature is above/below 1°C), an average value for all days with air temperature above/below 1°C was calculated, while for wind and relative humidity we calculated an average value for all observation days. These average values were used to generate time series of daily average input data to accelerate model spin-up required for permafrost to aggrade. Daily incoming shortwave radiation was modeled for one year based on latitude and day of year, for a slope of 0.1 and facing north, using methods by Kumar et al. (1997). The spin-up data time-series was repeated to generate data for 10.7 years (ending on September 17th). Observed daily data of air temperature, liquid precipitation, relative humidity, and wind speed from September 18, 2015 to August 17, 2017 from the SFT1 station were used to run simulations after spin-up (Figure S1). As the SFT1 station only records liquid precipitation, the average daily precipitation from the Asik station was used for snow days (air temperature <1°C) for both spin-up and subsequent simulations. The modeled incoming shortwave radiation data used for the spin-up was used also for the simulations with observed daily data.

3.6. Initialization

One-dimensional (1D) column model representations were used to generate initial pressure conditions for all model cases. For the continuous permafrost case, the 1D column was later frozen using a bottom boundary temperature of −2.5°C for 100 years. The 1D column pressure (all cases) and temperature (continuous permafrost case) results were draped on the 2D domain, and simulations were run (permafrost free and continuous permafrost cases) for 10 years to achieve cyclic steady-state in subsurface hydrology. For the discontinuous permafrost case, the 2D model was first run with an uneven distribution of incoming snow, to build up permafrost in the middle of the domain, following the methods of Jafarov et al. (2018). The same total amount of snow was put in the domain as in the two other cases, but distributed so that the snow cover from x = 400 to x = 800 m had half the thickness of the snow cover on the rest of the domain surface. This setup was used for the spin-up only, to create winter surface temperature that could create discontinuous permafrost in the domain. ATS uses a variable time step that adapts to limit the change in the solution variables. A maximum time step of 3h was also imposed for all simulations, but the maximum is typically only reached in the winter when the subsurface is completely frozen.

3.7. Sensitivity to Soil Hydraulic Properties

Additional simulations with modified soil hydraulic properties were performed for the permafrost-free and continuous permafrost cases to evaluate the effects of the surface organic horizon on model output. The soil hydraulic properties (permeability, water retention parameters, and porosity) of the peat layer were changed to the same as those of the mineral layers (Table 2). Spinup and simulation procedures followed the same as those for the original parameter setup but including these modified hydraulic properties settings. The simulations were run for testing the sensitivity of the results to the soil parameter setup, with regards to water partitioning, flow path, and temperature.

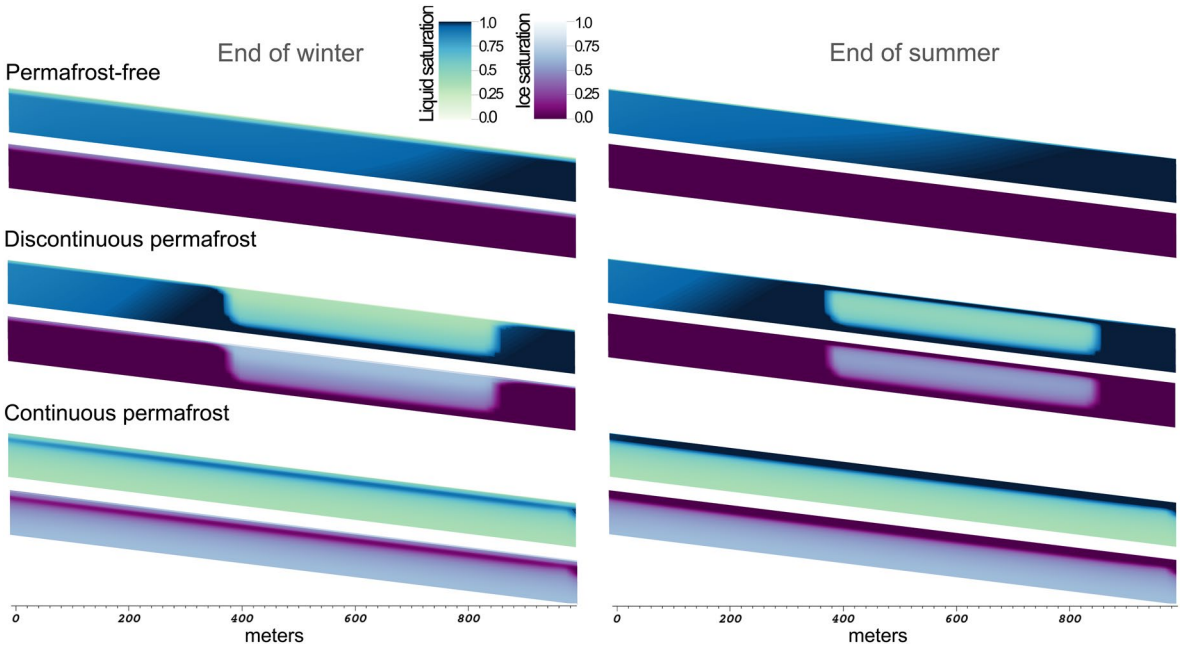


Figure 4. Liquid and ice saturation for the modeled cases after spin-up, at the start of snowmelt on May 5th (left) and at maximum active layer thickness, on October 10th (right). (Note that the geometry is modified to optimize visualization of the results, which causes the groundwater table to appear tilted upslope.).

3.8. Output Analysis

To quantify differences in magnitude for different flow pathways for the modeled hillslope cases, the horizontal component of the groundwater Darcy velocity was derived as averages for each of the soil layers. This average Darcy velocity was multiplied by the layer thickness to get a measure of the groundwater discharge in the horizontal direction for each layer. We focus on the horizontal component, as the vertical component mainly reflects infiltration processes. We include all cells in each layer in the calculations, whether saturated, unsaturated, or frozen, as saturation and freeze/thaw conditions will determine the overall movement of water across the hillslope.

To calculate the temperature of groundwater discharging from the domain, daily temperature and discharge values were output for each of the soil layers for the cells at the right side (downhill) boundary. The daily temperature of the total groundwater discharge from the right-side boundary was calculated by summing the temperatures scaled by the proportions of total discharge from all layers. One-year time-series of degree-days of groundwater discharge were calculated by cumulatively summing the positive daily temperatures for one year.

4. Simulation Results

There are major differences in the distribution of ice and liquid water between the three cases after spin-up. Most of the slope of the permafrost-free case is unsaturated, during both the winter and the summer (Figure 4). At the end of summer, a saturated zone extends from the bottom of the domain at around x = 550 m to the near surface at x = 850 m. The discontinuous permafrost case has permafrost extending from x = 390 m to x = 850 m, with a 1.2 m unfrozen zone beneath it and an active layer of 1.35 m. A saturated zone extends from upslope of the permafrost zone, through the active layer and below the permafrost. The continuous permafrost case has an active layer thickness of 1.67 m, and permafrost extending to bottom of the domain. The active layer has a saturated zone extending almost to the top of the hillslope during most of the summer.

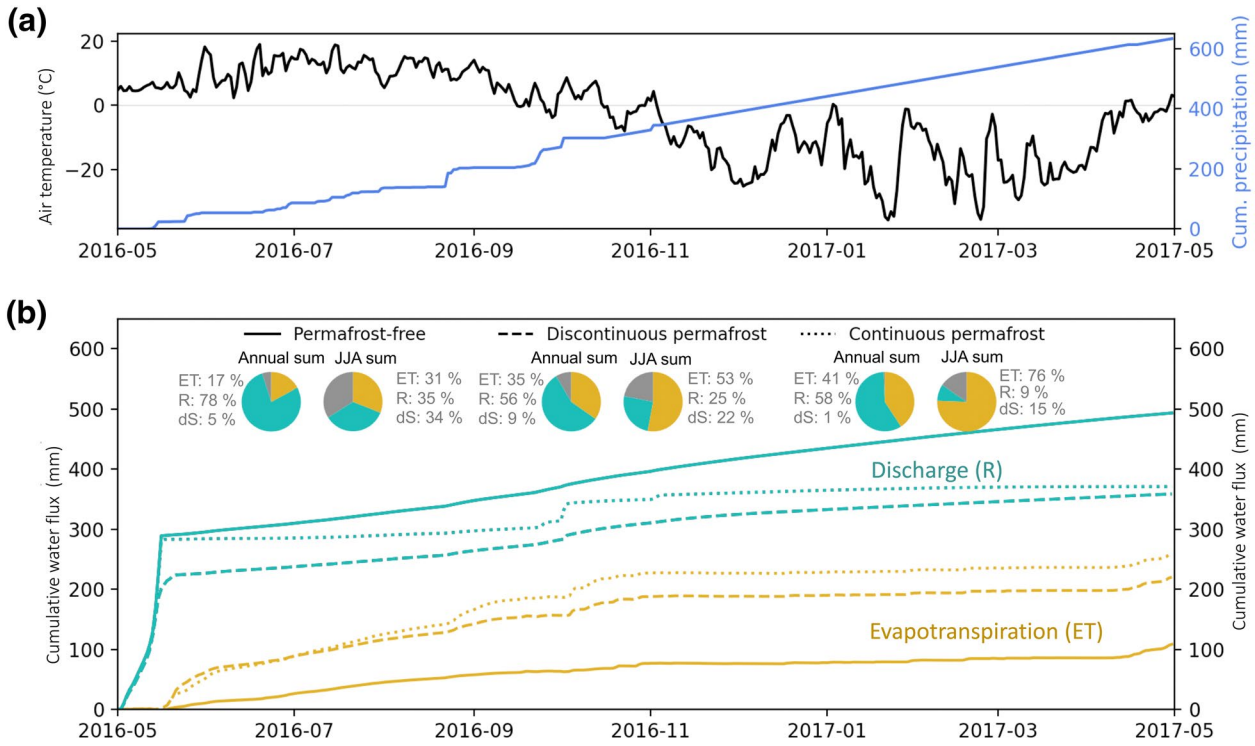


Figure 5. Air temperature and cumulative precipitation (P) used in the model (a), sum of surface and subsurface discharge (R) through the right (downhill) side boundary and evapotranspiration (ET) for each of the simulated cases (b). The pie graphs reflect shifting magnitude of total surface and subsurface discharge, evapotranspiration, and storage change (dS = P–ET–R) across the three permafrost scenarios for the full year and for the June, July, and August (JJA) period.

Permafrost conditions were a primary control on the amount and timing of water fluxes from the domain. Water budgets for the year May 1, 2016 to May 1, 2017 are presented for the three cases (Figure 5). As a reference, a total precipitation of 634 mm, of which 331 mm was snow, was put into the model for this year. The cumulative sum of surface and subsurface discharge as well as cumulative evapotranspiration varied across the three permafrost scenarios (Figure 5b). All of the cases exhibit a pronounced surface discharge peak at the spring freshet. For the remainder of the year, the permafrost-free case has a higher discharge and lower evapotranspiration compared to the discontinuous and continuous permafrost cases. The total annual evapotranspiration for the discontinuous permafrost case (220 mm) is double that for the permafrost-free case (108 mm), while for the continuous permafrost case it is even higher (259 mm). For the year presented, there was an increase in storage of 32 mm for the permafrost-free case, 55 mm for the discontinuous permafrost case, and 4 mm for the continuous permafrost case. For the June–August period (JJA) when no overland flow occurs, the continuous permafrost case has more than twice as much evapotranspiration as the permafrost-free case and only about a quarter of the amount of (groundwater) discharge.

The average horizontal water flux for each of the soil layers, as well as for overland flow, reveal key consistencies, and differences across permafrost scenarios (Figure 6). For all cases, overland flow dominates on an annual basis, due to the very high overland flow rates during the snowmelt event. The discontinuous and continuous permafrost cases also have high overland flow rates generated by rainfall events in the fall. For most of the year, however, there is no overland flow and water moves down the hillslopes through subsurface pathways. In the permafrost-free case, most of the groundwater moves through the mineral soil layers while with increasing permafrost, more water moves through the shallower organic soil layers. In the permafrost-free case, only 0.5% of the total annual flux moves through the organic soil layers (moss and peat), while in the discontinuous permafrost this number is 3.8%, and for the continuous permafrost case it is 6.7% of the total horizontal flux. The flux through the mineral layers corresponds to 45%, 32% and 13% of the annual horizontal flux for the permafrost-free, discontinuous, and continuous cases, respectively. For the

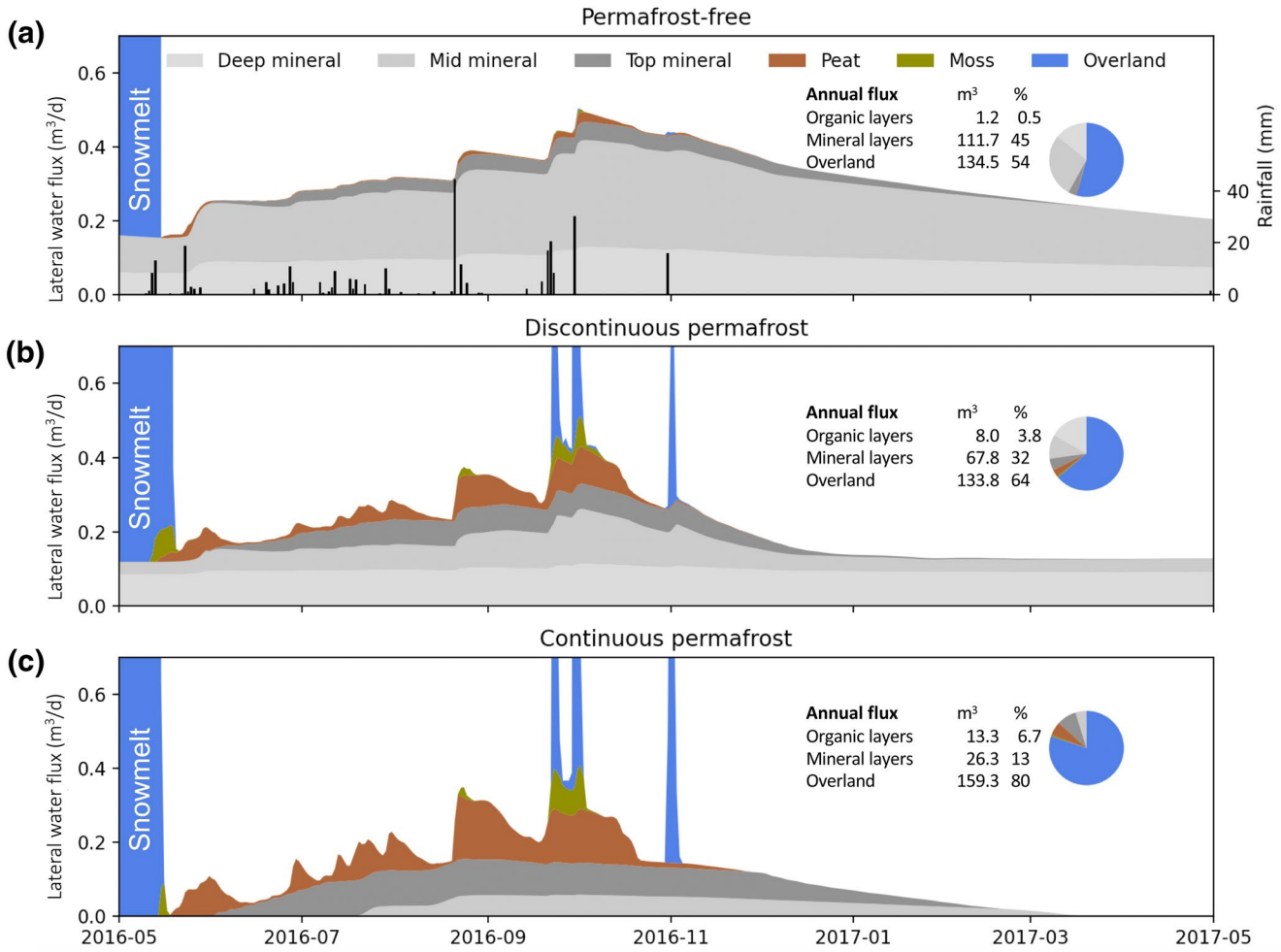


Figure 6. Lateral groundwater flux through each soil layer for the permafrost-free (a), discontinuous permafrost (b), and continuous permafrost cases (c), derived from the average velocity in the x-direction for each layer, multiplied by the layer thickness. Rainfall events (for all cases) are shown on the right y-axis of panel (a). The y-axis is truncated at 0.7 m^3/d, to clearly visualize the dynamics in the groundwater fluxes. Pie charts show the annual sums for flux through each layer and each modeling case.

continuous permafrost case, the groundwater discharge ceases entirely in March, reflecting complete freezing of the active layer, while there is groundwater discharge throughout the winter for the permafrost-free and discontinuous permafrost cases.

Permafrost presence and subsequently the depth of flow impacts the magnitude and temperature of the groundwater discharging through the downhill (right) boundary (Figure 7). The permafrost-free case has the highest groundwater discharge for all seasons, and the continuous permafrost case has the lowest. The greatest variation in discharge temperature over the year is found in the continuous permafrost case, from near 0°C in the winter to above 12°C in July, when temperatures peak. In July, the average simulated groundwater discharge temperatures are 4.0°C, 5.0°C, and 11.1°C for the permafrost-free, discontinuous permafrost, and continuous permafrost cases, respectively. The differences in seasonal temperature patterns is reflected in the accumulated degree days of the groundwater discharge over the year (Figure 7c). The continuous permafrost case rapidly accumulates degree days in the summer, but not at all during winter. By contrast, the permafrost-free case keeps accumulating degree days at a relatively slow rate over the whole year, although at a slower rate during the spring. The more stable temperature of the permafrost-free case over the year is due to the higher contribution of groundwater from deeper soil layers in which seasonal temperature variations are dampened. During times when overland flow occurs in the simulations, the temperatures of the overland water will impact and often dominate the total discharge temperature. However,

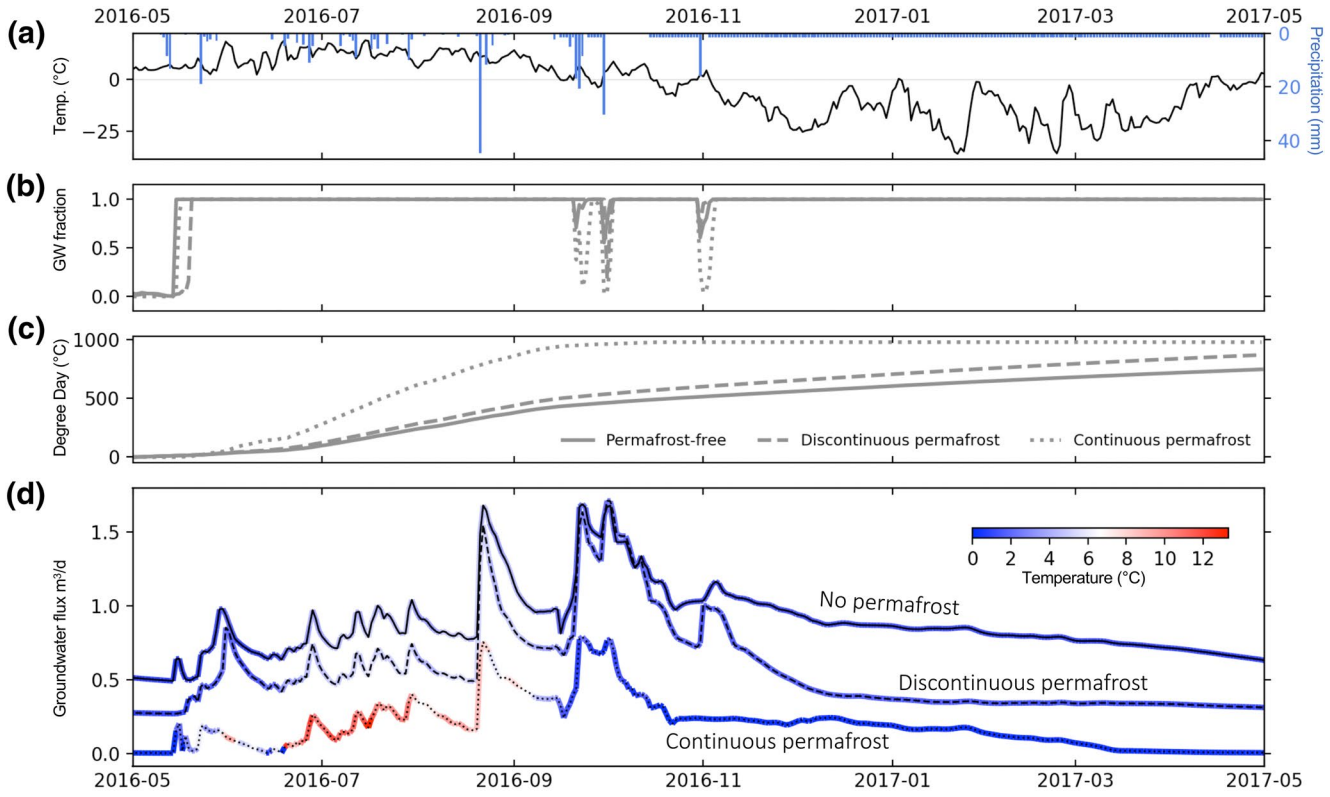


Figure 7. Daily air temperature and precipitation (a), groundwater as a fraction of total discharge from domain (b, 1 = only groundwater discharge, 0 = only surface water discharge), accumulated degree days of discharging groundwater (c), and magnitude of groundwater discharge colored by temperature (d).

our model was not optimized to represent the processes that control temperatures of water following such rapid flow pathways in detail, and the temperature of overland flow is therefore not further analyzed. There is no surface water discharge at the right-side boundary during the summer months, when water temperatures peak.

A sensitivity analysis using simulations with modified hydraulic properties of the peat layer (depth: 5–25 cm) resulted in minor changes to the water balance for the permafrost-free and continuous permafrost cases (Table S2). On the annual scale, none of the water balance components changed by more than 2% for either of the two simulation cases. For the JJA period discharge decreased from 35% to 31% for the permafrost-free case, and from 9% to 6% for the continuous permafrost case. This change was balanced by an increase in evapotranspiration (from 31% to 35%) for the permafrost-free case, and by a positive storage change in the continuous permafrost case. Flow through the top layers (moss and peat) for the permafrost-free case increased marginally from 0.5% to 0.6% of annual lateral flux, while for the continuous permafrost case it was more than cut by half from 6.7% to 3.1% of the annual lateral flux. The impact of this reduction in flow through the top layers on groundwater discharge temperatures was small relative to the impact of including continuous permafrost (Figures S2 and S3). The average simulated groundwater discharge temperature for July changed from 4.0°C to 2.8°C for the permafrost-free case, and from 11.1°C to 11.3°C for the continuous permafrost case. The warmer temperatures of groundwater discharge for the permafrost-free case with the original parameterization is mainly due to the seasonal frost layer creating a perched aquifer in the relatively warm top meter of the soil at the bottom of the slope. The slight increase in temperature for continuous permafrost case even though flow through the near-surface layers is dramatically reduced is likely related to a change in water table. With the modified hydraulic properties, the water table is located within the top 10 cm of most of the model domain in July, while in the original simulations the water table is generally found at 10–20 cm depth during the same time (Figure S4). This means that in the modified simulations,

less water is routed through the peat layer but this water is moving closer to the surface, where temperatures are higher.

5. Discussion

5.1. Permafrost Influences Hillslope Hydrology and Groundwater Temperatures

Our generic modeling results highlight considerable differences in hydrology across hillslopes with varying permafrost configurations. Implications of these results for headwater stream ecosystems in our study area are potentially substantial because wide-spread permafrost thaw is expected in the region. Air temperatures are projected to increase by 3.0–8.3°C in the Noatak National Preserve during the 21st century (Gonzalez et al., 2018). By the year 2100, the permafrost in our larger study region is projected to transition from continuous (>90% of land area) to discontinuous coverage (50%–90%), and specifically for the Agashashok and Cutler-Imelyak catchments studied here, most are projected to be free of near-surface permafrost by 2100 (Panda et al., 2016). The simulation cases are therefore in the range of expected future changes in permafrost, and the results suggest the potential effects of thaw on hydrology and stream ecosystems.

Flow paths are drastically affected by permafrost extent in our simulations, which is consistent with prior modeling and observation-based studies (Evans & Ge, 2017; Frampton & Destouni, 2015; O'Donnell et al., 2014; Walvoord et al., 2019). The flow through the organic layer is more than 10 times higher in our simulated continuous permafrost case, compared to the permafrost-free case. During the summer, rainfall events trigger lateral flow in both mineral and organic layers in the two permafrost cases, while in the permafrost-free case mainly mineral soil flow paths are activated. Such triggering of flow through the organic layers is consistent with observations from a discontinuous permafrost headwater catchment in Alaska, and to some extent with data from Yukon although high uncertainty was associated with these field-based quantifications of flow path partitioning (S. K. Carey & Quinton, 2005; Koch et al., 2014). When the active layer freezes in the winter, groundwater discharge to streams ceases with continuous permafrost. As our simulated active layer thickness (~1.3 m) is deeper than what we have observed at some of our sites (~0.6–1.0 m, Koch, O'Donnell, & Carey, 2020), but in the range of active layer thickness simulated for the region (0.5–1.5 m) by Panda et al. (2016), these results can be considered conservative in terms of flow path depth. Without permafrost, flow paths are deeper, and streams in permafrost-free terrain receive groundwater input in all seasons (Figure 7d). These differences in flow path depths will likely influence water cycling and quality in headwater catchments.

One important implication of differences in subsurface flow depth is the somewhat counter-intuitive impact on water temperature. Near-surface soil layers will warm considerably in the summer due to incoming solar radiation and warmer air temperatures even where permafrost is present at depth (Smith et al., 2010). In combination with higher hydraulic conductivity in the upper soil layers (Quinton et al., 2000), the shallow flow paths that dominate when continuous permafrost limits infiltration generate a high proportion of relatively warm groundwater discharge during the summer. The effect of this mechanism is clearly seen in our modeling results, and offers an explanation to the stream temperatures observed in our Alaskan headwater catchments (Figure 2). In our simulations, the temperatures in the active layer are similar between the three cases due to all cases being run with the same climate input data. The simulated ground temperatures are also within the ranges of observed temperatures in the top 0.5 m of the ground, during the summer (Figure S5). Our sensitivity analysis indicates that this trend is independent of peat soil properties.

5.2. Stream Temperature Complexity

Our modeling results suggest an explanation to the observed pattern of warmer summer stream temperatures in permafrost-rich headwater catchments. Despite short water transit times for the headwater streams we have studied (on the scale of 1 day), in-stream processes such as warming from incoming shortwave radiation, are likely to de-couple stream temperatures from groundwater discharge temperatures to some extent (Caissie, 2006). Our simulations were not aimed at reproducing temperature dynamics controlled by in-stream processes, but rather at investigating the potential effect of permafrost on the temperature

of groundwater that may serve as a stream water source. Warming from incoming radiation is the dominant source of energy to most streams (Cozzetto et al., 2006; Zheng et al., 2019) and shading is limited in our systems due to minimal canopy cover, leading to higher observed median and maximum stream temperatures than the simulated groundwater discharge temperatures. This should theoretically result in high daily maximum temperatures and diurnal temperature ranges, and general warming of stream water (Caissie, 2006; Sinokrot & Stefan, 1993). While observed minimum stream temperatures ranged from 6.5°C to 11.5°C our simulated groundwater discharge temperatures were lower, ranging from 4.0°C to 11.1°C for July, supporting the idea of limited in-stream warming. We find no significant trend of increasing diurnal temperature range with permafrost cover or with south-facing slope aspect (Figure S6), which suggests that differences in shading (although difficult to quantify entirely along streams) are not the main cause of the observed pattern in stream temperatures. The fact that our regressions between temperature and permafrost cover persist regardless of whether we look at minimum, median, or maximum temperature suggests that the variation in temperature of the incoming groundwater may be dominating over in-stream warming in these streams. Although the aim of this study was not to fully disentangle effects of in-stream processes and groundwater discharge on stream temperatures in our headwater catchments, the empirical data provide compelling support for our simulation results.

5.3. Changing Arctic Ecosystems

Sensitivities of stream temperatures to warming air temperature have previously been investigated using both empirical and mechanistic approaches, but have been mainly restricted to permafrost-free areas (Kelleher et al., 2012; Leach & Moore, 2019; Lisi et al., 2015; Piccolroaz et al., 2016). Mechanistic models that account for groundwater contributions to streams have shown that temperatures of groundwater discharge will increase with the air temperature (Kurylyk et al., 2014; Leach & Moore, 2019; Snyder et al., 2015). For example, a ~1°C/°C increase in mean August stream temperature with air temperature increase was estimated in simulations for a permafrost-free forested headwater catchment in British Columbia (Leach & Moore, 2019). Countering this, our simulations indicate that permafrost thaw-driven changes in flow paths will lead to colder groundwater discharge temperatures in the summer, without including changes in air temperature.

Altered discharge flow paths may lead to water quality changes that impact stream ecosystems. Our results show that permafrost impacts the magnitude, timing, temperature, and depth of runoff, which control surface water quality (O'Donnell et al., 2016; Striegl et al., 2005; Toohey et al., 2016; Vonk et al., 2015) and possibly food web dynamics (O'Donnell et al., 2019). Stream temperature is a critical water quality variable for aquatic ecosystems and specifically for fish survival, growth, and reproduction (M. P. Carey & Zimmerman, 2014; Hughes, 1998; Magnuson et al., 1990; Nielsen et al., 2013; Reist et al., 2006; Shuter et al., 2012). In fact, temperature is the primary determinant of fish production and survival influencing metabolic demands and lethal temperatures. As such, our results suggest that permafrost thaw-driven changes in groundwater flow paths may reduce fish growth in headwater streams by providing cooler summer water temperatures. Lower summer growth likely reduces juvenile survival with potential consequences for the fish populations (Childress et al., 2019). In contrast, as the depth of subsurface flow paths increase, we may see a shift from organic nutrients (e.g., dissolved organic nitrogen or phosphorus) toward inorganic nutrients (e.g., nitrate and phosphate), which are more easily assimilated by stream biota and incorporated into food webs and fish through bottom-up processes (Deegan et al., 1997).

The projected changes in climate and permafrost thaw will be accompanied by changes in vegetation that will likely have further impact on flow paths and the discharge and thermal responses of streams (Pastick et al., 2014). Observed changes in vegetation productivity suggest that plants are already using increasing amounts of water in some areas of Alaska, while in other areas, drought stress can lead to decreasing vegetation productivity (Pastick et al., 2019). In our study area, migration of the tree line, which cuts through our catchments, can lead to more shading by trees along streams, reducing the warming effect of incoming shortwave radiation. However, deepening of catchment flow paths may eventually limit trees to the riparian corridors. Furthermore, with deeper flow paths, groundwater recharge may bypass headwater streams,

leading to drying (Walvoord et al., 2012). The net effect of increasing air temperatures on stream water discharge and temperatures is therefore not easily quantified.

Changes in vegetation also bring changes in transpiration—a process that is not well-represented in our simulations. In Arctic climates, evapotranspiration is rarely limited by water availability, and evaporation often dominates over transpiration (Young-Robertson et al., 2018). Consequently, representing evapotranspiration using models limited through soil availability has proven sufficient in previous modeling studies in Arctic settings (Jan et al., 2020). Rather than the simplified representation of transpiration, the geometry of our simulated hillslopes might limit annual evapotranspiration rates in comparison with catchment-scale fluxes, because it generates rapid surface runoff during the snowmelt and lacks regional groundwater discharge areas. Considering only the summer period when no overland flow occurs in our simulations, evapotranspiration constitutes 31%–76% of input precipitation in the simulated cases and simulated runoff ratios (runoff/precipitation) for the summer are in the range of observed values in permafrost-affected catchments (Koch, Runkel, et al., 2013; Stuefer et al., 2017; Yamazaki et al., 2006). Our results show that evapotranspiration rates are dramatically reduced from continuous to permafrost free conditions—cut in half on an annual scale—due to deeper infiltration and drying of near-surface soils. Plants with deep roots could access and transpire water from deeper soil layers, yielding higher evapotranspiration rates than in our simulated permafrost-free scenario (Orgogozo et al., 2019). However, micrometeorological observations from Alaska indicate that evapotranspiration rates are similar between tundra and forest sites and that mainly the partitioning between transpiration and evaporation that differs (Beringer et al., 2005). Neglecting such vegetation-driven effects and isolating the effects of permafrost presence, our results show great impact on evapotranspiration rates with permafrost thaw.

5.4. Remaining Uncertainties

In our model we have isolated the effects of permafrost on hillslope hydrology, while in reality permafrost is one of many interacting factors controlling changes in Arctic ecosystems. To further our understanding of the trajectories of Arctic headwater catchments with warming and thaw, some inherent uncertainties should be addressed. First of all, the combined effect of transient changes in air temperature, precipitation, permafrost and vegetation remains to be investigated, and is likely to impact the partitioning of precipitation into evapotranspiration and runoff, and thereby flow path distribution and temperatures of groundwater discharge. Second, while our simple 2D geometry allowed for direct comparison of flow paths between model cases, our model results are not directly translatable to catchment-scale understanding due to the simplified geometry. Microtopography, which was not represented, could impact overland flow retention—especially during and following snowmelt—and thereby the partitioning of infiltration and evapotranspiration in the early summer. On a larger scale, the control of permafrost on the locations of groundwater discharge areas to streams would be important to investigate for understanding catchment-scale validity of our results. Such larger scale understanding would likely be needed to more conclusively link observed stream water temperatures to flow path distributions. Third, across the Arctic permafrost areas, and within the region of our study, variability in soils, geology, ground ice conditions could also impact spatial and temporal patterns in hillslope groundwater flow paths. For example, thawing of low conductivity materials, such as unfractured bedrock, would likely result in minor effects of flow path distributions. Finally, the thermal response of streams and larger rivers to changes in groundwater temperatures following permafrost thaw is controlled by in-stream thermal processes not investigated here and motivates future research and monitoring of Arctic river systems.

6. Conclusions

Headwater streams in northwest Alaska had warmer July water temperatures with increasing near-stream permafrost cover. Based on our generic cryohydrology model experiment we suggest that the impact of permafrost on hillslope flow path depth can explain this pattern. The differences in hillslope hydrology between our three simulated cases—permafrost-free, discontinuous permafrost, and continuous permafrost—suggest that projected permafrost thaw will have considerable consequences for stream ecosystems.

Some of these consequences may seem counterintuitive, such as the fact that warming could lead to less evapotranspiration and colder stream summer temperatures due to permafrost thaw-induced changes in flow paths. High future warming scenarios and associated changes in vegetation could, however, counter this effect to some extent by increasing in-stream warming and transpiration from plants with deep roots. Nevertheless, these results show that response of high-latitude streams to a warming climate will be partially mediated by thaw-induced flow path changes. In addition to the effects on stream temperature and groundwater inflows addressed here, flow path changes potentially have important effects on water chemistry and, as a result from nutrients and temperature, fish populations in headwater streams.

Data Availability

Data used in the study are described and cited in the methods section, and available in the U.S. Geological Survey data releases by Koch et al. (2019), Koch, O'Donnell, and Carey (2020), Koch, Sjöberg, and Carey (2020), and Koch, Carey, et al. (2020) and M. P. Carey et al. (2020), and the Hill and Sousanes (2018) climate data release from the National Parks Service.

Acknowledgments
This research was funded by the Swedish Research Council for Environment, Agricultural Sciences and Spatial Planning (Formas) grant number 2015-00790 (Y. Sjöberg), and supported by the Changing Arctic Ecosystems Initiative of the Wildlife program of the U.S. Geological Survey Ecosystems Mission Area, and the National Park Service's Arctic Inventory and Monitoring Network and staff from the Western Arctic Parklands in Kotzebue, Alaska. Oak Ridge National Laboratory's contribution to this work was supported by the Next-Generation Ecosystem Experiment—Arctic (NGEE-Arctic) project. The NGEE-Arctic project is supported by the Office of Biological and Environmental Research in the U.S. Department of Energy's Office of Science. The simulations were performed on resources at Chalmers Centre for Computational Science and Engineering (C3SE) provided by the Swedish National Infrastructure for Computing (SNIC). For calculations of incoming solar radiation, based on latitude and day of year, a script by Felix Hebeler (available at https://www.mathworks.com/matlabcentral/fileexchange/19791-solar-radiation) was modified for the site conditions and study purposes. Meteorological data collection was supported by the Arctic Land Conservation Cooperative. All analyses of soil samples were conducted by the laboratory at Daniel B. Stephens & Associates, Inc. This manuscript benefitted greatly from reviews by Marty Briggs, Sean Carey, two anonymous reviewers, the USGS Office of Science Quality and Integrity, as well as the guidance from Associate Editor Dan Moore. Any use of trade, firm, or product names is for descriptive purposes only and does not imply endorsement by the U.S. Government.

References

Abolt, C. J., Young, M. H., Atchley, A. L., & Harp, D. R. (2018). Microtopographic control on the ground thermal regime in ice wedge polygons. *The Cryosphere*, *12*(6), 1957–1968. https://doi.org/10.5194/tc-12-1957-2018

ACIA. (2004). *Impacts of a warming Arctic: Arctic climate impact assessment*. Cambridge University Press. Retrieved from https://www.amap.no/documents/doc/impacts-of-a-warming-arctic-2004/786

Andresen, C. G., Lawrence, D. M., Wilson, C. J., McGuire, A. D., Koven, C., Schaefer, K., et al. (2020). Soil moisture and mydrology projections of the permafrost region—A model intercomparison. *The Cryosphere*, *14*, 445–459. https://doi.org/10.5194/tc-14-445-2020

Atchley, A. L., Coon, E. T., Painter, S. L., Harp, D. R., & Wilson, C. J. (2016). Influences and interactions of inundation, peat, and snow on active layer thickness. *Geophysical Research Letters*, *43*(10), 5116–5123. https://doi.org/10.1002/2016GL068550

Atchley, A. L., Painter, S. L., Harp, D. R., Coon, E. T., Wilson, C. J., Liljedahl, A. K., & Romanovsky, V. E. (2015). Using field observations to inform thermal hydrology models of permafrost dynamics with ATS (v0.83). *Geoscientific Model Development*, *8*(9), 2701–2722. https://doi.org/10.5194/gmd-8-2701-2015

Bense, V. F., Kooi, H., Ferguson, G., & Read, T. (2012). Permafrost degradation as a control on hydrogeological regime shifts in a warming climate. *Journal of Geophysical Research*, *117*(F3), F03036. https://doi.org/10.1029/2011JF002143

Beringer, J., Chapin, F. S., III, Thompson, C. C., & McGuire, A. D. (2005). Surface energy exchanges along a tundra-forest transition and feedbacks to climate. *Agricultural and Forest Meteorology*, *131*(3–4), 143–161. https://doi.org/10.1016/j.agrformet.2005.05.006

Bintanja, R., & Selten, F. M. (2014). Future increases in Arctic precipitation linked to local evaporation and sea-ice retreat. *Nature*, *509*(7501), 479–482. https://doi.org/10.1038/nature13259

Bring, A., Fedorova, I., Dibike, Y., Hinzman, L., Mård, J., Mernild, S. H., et al. (2016). Arctic terrestrial hydrology: A synthesis of processes, regional effects, and research challenges. *Journal of Geophysical Research: Biogeosciences*, *121*(3), 621–649. https://doi.org/10.1002/2015JG003131

Brown, J., Ferrians, O., Heginbottom, J. A., & Melnikov, E. (2002). *Circum-Arctic map of permafrost and ground-ice conditions version 2*. Boulder, CO: NSIDC: National Snow and Ice Data Center.

Caissie, D. (2006). The thermal regime of rivers: A review. *Freshwater Biology*, *51*(8), 1389–1406. https://doi.org/10.1111/j.1365-2427.2006.01597.x

Canadell, J., Jackson, R. B., Ehleringer, J. B., Mooney, H. A., Sala, O. E., & Schulze, E.-D. (1996). Maximum rooting depth of vegetation types at the global scale. *Oecologia*, *108*, 583–595. https://doi.org/10.1007/BF00329030

Carey, M. P., Koch, J. C., O'Donnell, J. A., & Sjöberg, Y. (2020). *Stream temperatures in the Noatak River and Kobuk River basins, Northwest Alaska, 2017–2019*, Anchorage: U.S. Geological Survey Data Release. https://doi.org/10.5066/P91HI62H

Carey, S. K., & Quinton, W. L. (2005). Evaluating runoff generation during summer using hydrometric, stable isotope and hydrochemical methods in a discontinuous permafrost alpine catchment. *Hydrological Processes*, *19*, 95–114. https://doi.org/10.1002/hyp.5764

Carey, M. P., & Zimmerman, C. E. (2014). Physiological and ecological effects of increasing temperature on fish production in lakes of Arctic Alaska. *Ecology and Evolution*, *4*(10), 1981–1993. https://doi.org/10.1002/ece3.1080

Chadburn, S. E., Burke, E. J., Cox, P. M., Friedlingstein, P., Hugelius, G., & Westermann, S. (2017). An observation-based constraint on permafrost loss as a function of global warming. *Nature Climate Change*, *7*(5), 340–344. https://doi.org/10.1038/nclimate3262

Childress, E. S., Nislow, K. H., Whiteley, A. R., O'Donnell, M. J., & Letcher, B. H. (2019). Daily estimates reveal fine-scale temporal and spatial variation in fish survival across a stream network. *Canadian Journal of Fisheries and Aquatic Sciences*, *76*(8), 1446–1458. https://doi.org/10.1139/cjfas-2018-0191

Coon, E. T., Berndt, M., Jan, A., Svyatskiy, D., Atchley, A. L., Kikinzon, E., et al. (2019). *Advanced terrestrial simulator 0.88*, Washington DC: U.S. Department of Energy. https://doi.org/10.11578/dc.20190911.1

Cozzetto, K., McKnight, D., Nylen, T., & Fountain, A. (2006). Experimental investigations into processes controlling stream and hyporheic temperatures, Fryxell Basin, Antarctica. *Advances in Water Resources*, *29*(2), 130–153. https://doi.org/10.1016/j.advwatres.2005.04.012

Creed, I. F., Bergström, A.-K., Trick, C. G., Grimm, N. B., Hessen, D. O., Karlsson, J., et al. (2018). Global change-driven effects on dissolved organic matter composition: Implications for food webs of northern lakes. *Global Change Biology*, *24*(8), 3692–3714. https://doi.org/10.1111/gcb.14129

Deegan, L. A., Peterson, B. J., Golden, H., McIvor, C. C., & Miller, M. C. (1997). Effects of fish density and river fertilization on algal standing stocks, invertebrate communities, and fish production in an arctic river. *Canadian Journal of Fisheries and Aquatic Sciences*, *54*(2), 269–283. https://doi.org/10.1139/f96-268

Endrizzi, S., Gruber, S., Dall&apos, Amico, M., & Rigon, R. (2014). GEOtop 2.0: simulating the combined energy and water balance at and below the land surface accounting for soil freezing, snow cover and terrain effects. *Geoscientific Model Development*, *7*(6), 2831–2857. https://doi.org/10.5194/gmd-7-2831-2014

Evans, S. G., & Ge, S. (2017). Contrasting hydrogeologic responses to warming in permafrost and seasonally frozen ground hillslopes. *Geophysical Research Letters*, *44*(4), 1803–1813. https://doi.org/10.1002/2016GL072009

Fabris, L., Rolick, R. L., Kurylyk, B. L., & Carey, S. K. (2020). Characterization of contrasting flow and thermal regimes in two adjacent subarctic alpine headwaters in Northwest Canada. *Hydrological Processes*, *34*, 3252–3270. https://doi.org/10.1002/hyp.13786

Frampton, A., & Destouni, G. (2015). Impact of degrading permafrost on subsurface solute transport pathways and travel times. *Water Resources Research*, *51*(9), 7680–7701. https://doi.org/10.1002/2014WR016689

Frampton, A., Painter, S. L., & Destouni, G. (2013). Permafrost degradation and subsurface-flow changes caused by surface warming trends. *Hydrogeology Journal*, *21*(1), 271–280. https://doi.org/10.1007/s10040-012-0938-z

Gonzalez, P., Wang, F., Notaro, M., Vimont, D. J., & Williams, J. W. (2018). Disproportionate magnitude of climate change in United States national parks. *Environmental Research Letters*, *13*(10), 104001. https://doi.org/10.1088/1748-9326/aade09

Hamilton, T. D. (2010). *Surficial geologic map of the Noatak National Preserve*, Anchorage: U.S Geological Survey Scientific Investigations Map.

Hansen, J., Ruedy, R., Glascoe, J., & Sato, M. (1999). GISS analysis of surface temperature change. *Journal of Geophysical Research*, *104*(D24), 30997–31022. https://doi.org/10.1029/1999JD900835

Harp, D. R., Atchley, A. L., Painter, S. L., Coon, E. T., Wilson, C. J., Romanovsky, V. E., & Rowland, J. C. (2016). Effect of soil property uncertainties on permafrost thaw projections: A calibration-constrained analysis. *The Cryosphere*, *10*(1), 341–358. https://doi.org/10.5194/tc-10-341-2016

Hill, K. H., Sousanes, P. J., & Miller, S. (2016). *2016 ARCN Weather and Climate Data Deliverables, National Park Service Arctic Inventory and monitoring network quality controlled climate dataset*. U.S National Park Service.

Hinzman, L. D., Bettez, N. D., Bolton, W. R., Chapin, F. S., Dyurgerov, M. B., Fastie, C. L., et al. (2005). Evidence and implications of recent climate change in northern Alaska and other Arctic regions. *Climatic Change*, *72*(3), 251–298. https://doi.org/10.1007/s10584-005-5352-2

Hughes, N. F. (1998). A model of habitat selection by drift-feeding stream salmonids at different scales. *Ecology*, *79*(1), 281–294. https://doi.org/10.1890/0012-9658(1998)079[0281:AMOHSB]2.0.CO2

Jafarov, E., Coon, E., Harp, D., Wilson, C. J., Painter, S., Atchley, A., & Romanovsky, V. (2018). Modeling the role of preferential snow accumulation in through talik development and hillslope groundwater flow in a transitional permafrost landscape. *Environmental Research Letters*, *13*, 105006. https://doi.org/10.1088/1748-9326/aadd30

Jan, A., Coon, E., & Painter, S. L. (2020). Evaluating integrated surface/subsurface permafrost thermal hydrology models in ATS (v0.88) against observations from a polygonal tundra site. *Geoscientific Model Development*, *13*, 2259–2276. https://doi.org/10.5194/gmd-13-2259-2020

Jan, A., Coon, E. T., Painter, S. L., Garimella, R., & Moulton, J. D. (2018). An intermediate-scale model for thermal hydrology in low-relief permafrost-affected landscapes. *Computational Geosciences*, *22*(1), 163–177. https://doi.org/10.1007/s10596-017-9679-3

Jorgenson, M. T., Roth, J. E., Miller, P. F., Macander, M. J., Duffy, M. S., Wells, A. F., et al. (2009). *An ecological land survey and landcover map of the Arctic Network* (Natural Resource Technical Report NPS/ARCN/NRTR-2009/270). U.S. National Park Service.

Kelleher, C., Wagener, T., Gooseff, M., McGlynn, B., McGuire, K., & Marshall, L. (2012). Investigating controls on the thermal sensitivity of Pennsylvania streams. *Hydrological Processes*, *26*(5), 771–785. https://doi.org/10.1002/hyp.8186

Kendrick, M. R., Huryn, A. D., Bowden, W. B., Deegan, L. A., Findlay, R. H., Hershey, A. E., et al. (2018). Linking permafrost thaw to shifting biogeochemistry and food web resources in an arctic river. *Global Change Biology*, *24*(12), 5738–5750. https://doi.org/10.1111/gcb.14448

King, T. V., Neilson, B. T., Overbeck, L. D., & Kane, D. L. (2016). Water temperature controls in low arctic rivers. *Water Resources Research*, *52*, 4358–4376. https://doi.org/10.1002/2015WR017965

Koch, J. C., Carey, M. P., & O'Donnell, J. A. (2019). *Water level, temperature, and discharge of headwater streams in the Noatak and Kobuk River Basins, Northwest Alaska, 2015–2017*, Anchorage: U.S. Geological Survey Data Release. https://doi.org/10.5066/P9EIX8ET

Koch, J. C., Carey, M. P., O'Donnell, J. A., & Hill, K. (2020). *Meteorological data from two locations in the Agashashok River watershed, Northwestern Alaska, 2015 to 2017*, Anchorage: U.S. Geological Survey Data Release. https://doi.org/10.5066/P9HRDPDY

Koch, J. C., Ewing, S. A., Striegl, R., & McKnight, D. M. (2013). Rapid runoff via shallow throughflow and deeper preferential flow in a boreal catchment underlain by frozen silt (Alaska, USA). *Hydrogeology Journal*, *21*(1), 93–106. https://doi.org/10.1007/s10040-012-0934-3

Koch, J. C., Kikuchi, C. P., Wickland, K. P., & Schuster, P. (2014). Runoff sources and flow paths in a partially burned, upland boreal catchment underlain by permafrost. *Water Resources Research*, *50*, 8141–8158. https://doi.org/10.1002/2014WR015586

Koch, J. C., O'Donnell, J. A., & Carey, M. P. (2020). *Continuous records of shallow soil temperature and moisture in the Noatak River Basin, Alaska*, Anchorage: U.S. Geological Survey Data Release. https://doi.org/10.5066/P9048PDL

Koch, J. C., Runkel, R. L., Striegl, R., & McKnight, D. M. (2013). Hydrologic controls on the transport and cycling of carbon and nitrogen in a boreal catchment underlain by continuous permafrost. *Journal of Geophysical Research: Biogeosciences*, *118*(2), 698–712. https://doi.org/10.1002/jgrg.20058

Koch, J. C., Sjöberg, Y., & Carey, M. P. (2020). *Physical, hydraulic, and thermal properties of soils in the Noatak River Basin, Alaska, 2016*, Anchorage: U.S. Geological Survey Data Release. https://doi.org/10.5066/P9C3JYUH

Koven, C. D., Riley, W. J., Stern, A., Koven, C. D., Riley, W. J., & Stern, A. (2013). Analysis of permafrost thermal dynamics and response to climate change in the CMIP5 earth system models. *Journal of Climate*, *26*(6), 1877–1900. https://doi.org/10.1175/JCLI-D-12-00228.1

Kumar, L., Skidmore, A. K., & Knowles, E. (1997). Modelling topographic variation in solar radiation in a GIS environment. *International Journal of Geographical Information Science*, *11*(5), 475–497. https://doi.org/10.1080/136588197242266

Kurylyk, B. L., Hayashi, M., Quinton, W. L., McKenzie, J. M., & Voss, C. I. (2016). Influence of vertical and lateral heat transfer on permafrost thaw, peatland landscape transition, and groundwater flow. *Water Resources Research*, *52*(2), 1286–1305. https://doi.org/10.1002/2015WR018057

Kurylyk, B. L., MacQuarrie, K. T. B., & Voss, C. I. (2014). Climate change impacts on the temperature and magnitude of groundwater discharge from shallow, unconfined aquifers. *Water Resources Research*, *50*(4), 3253–3274. https://doi.org/10.1002/2013WR014588

Lammers, R. B., Pundsack, J. W., & Shiklomanov, A. I. (2007). Variability in river temperature, discharge, and energy flux from the Russian Pan-Arctic landmass. *Journal of Geophysical Research*, *112*, G04S59. https://doi.org/10.1029/2006JG000370

Lamontagne-Hallé, P., McKenzie, J. M., Kurylyk, B. L., & Zipper, S. C. (2018). Changing groundwater discharge dynamics in permafrost regions. *Environmental Research Letters*, *13*(8), 084017. https://doi.org/10.1088/1748-9326/aad404

Leach, J. A., & Moore, R. D. (2019). Empirical stream thermal sensitivities may underestimate stream temperature response to climate warming. *Water Resources Research*, *55*(7), 5453–5467. https://doi.org/10.1029/2018WR024236

Lisi, P. J., Schindler, D. E., Cline, T. J., Scheuerell, M. D., & Walsh, P. B. (2015). Watershed geomorphology and snowmelt control stream thermal sensitivity to air temperature. *Geophysical Research Letters*, *42*(9), 3380–3388. https://doi.org/10.1002/2015GL064083

Magnuson, J. J., Meisner, J. D., & Hill, D. K. (1990). Potential changes in the thermal habitat of Great Lakes fish after global climate warming. *Transactions of the American Fisheries Society*, *119*(2), 254–264. https://doi.org/10.1577/1548-8659(1990)119<0254:PCITTH>2.3.CO;2

McKenzie, J. M., & Voss, C. I. (2013). Permafrost thaw in a nested groundwater-flow system. *Hydrogeology Journal*, *21*(1), 299–316. https://doi.org/10.1007/s10040-012-0942-3

Nielsen, J. L., Ruggerone, G. T., & Zimmerman, C. E. (2013). Adaptive strategies and life history characteristics in a warming climate: Salmon in the Arctic? *Environmental Biology of Fishes*, *96*(10–11), 1187–1226. https://doi.org/10.1007/s10641-012-0082-6

Orgogozo, L., Prokushkin, A. S., Pokrovsky, O. S., Grenier, C., Quintard, M., Viers, J., & Audry, S. (2019). Water and energy transfer modeling in a permafrost-dominated, forested catchment of Central Siberia: The key role of rooting depth. *Permafrost and Periglacial Processes*, *30*(2), 75–89. https://doi.org/10.1002/ppp.1995

O'Connor, M. T., Cardenas, M. B., Neilson, B. T., Nicholaides, K. D., & Kling, G. W. (2019). Active layer groundwater flow: the interrelated effects of stratigraphy, thaw, and topography. *Water Resources Research*, *55*(8), 6555–6576. https://doi.org/10.1029/2018WR024636

O'Donnell, J. A., Aiken, G. R., Swanson, D. K., Panda, S., Butler, K. D., & Baltensperger, A. P. (2016). Dissolved organic matter composition of Arctic rivers: Linking permafrost and parent material to riverine carbon. *Global Biogeochemical Cycles*, *30*(12), 1811–1826. https://doi.org/10.1002/2016GB005482

O'Donnell, J. A., Aiken, G. R., Walvoord, M. A., Raymond, P. A., Butler, K. D., Dornblaser, M. M., & Heckman, K. (2014). Using dissolved organic matter age and composition to detect permafrost thaw in boreal watersheds of interior Alaska. *Journal of Geophysical Research: Biogeosciences*, *119*(11), 2155–2170. https://doi.org/10.1002/2014JG002695

O'Donnell, J. A., Carey, M. P., Koch, J. C., Xu, X., Poulin, B., Walker, J., & Zimmerman, C. E. (2019). Permafrost hydrology drives the assimilation of old carbon by stream food webs in the Arctic. *Ecosystems*, *23*, 435–453. https://doi.org/10.1007/s10021-019-00413-6

Painter, S. L., Coon, E. T., Atchley, A. L., Berndt, M., Garimella, R., Moulton, J. D., et al. (2016). Integrated surface/subsurface permafrost thermal hydrology: Model formulation and proof-of-concept simulations. *Water Resources Research*, *52*(8), 6062–6077. https://doi.org/10.1002/2015WR018427

Painter, S. L., & Karra, S. (2014). Constitutive model for unfrozen water content in subfreezing unsaturated soils. *Vadose Zone Journal*, *13*(4), vzj2013. https://doi.org/10.2136/vzj2013.04.0071

Panda, S. K., Romanovsky, V. E., & Marchenko, S. S. (2016). *High-resolution permafrost modeling in the Arctic network national parks, preserves and monuments*. (Natural Resource Report NPS/ARCN/NRR—2016/1366). Fort Collins, CO: National Park Service.

Pastick, N. J., Jorgenson, M. T., Goetz, S. J., Jones, B. M., Wylie, B. K., Minsley, B. J., et al. (2019). Spatiotemporal remote sensing of ecosystem change and causation across Alaska. *Global Change Biology*, *25*(3), 1171–1189. https://doi.org/10.1111/gcb.14279

Pastick, N. J., Jorgenson, M. T., Wylie, B. K., Rose, J. R., Rigge, M., & Walvoord, M. A. (2014). Spatial variability and landscape controls of near-surface permafrost within the Alaskan Yukon River Basin. *Journal of Geophysical Research Biogeosciences*, *119*, 1244–1265. https://doi.org/10.1002/2013JG002594

Piccolroaz, S., Calamita, E., Majone, B., Gallice, A., Siviglia, A., & Toffolon, M. (2016). Prediction of river water temperature: A comparison between a new family of hybrid models and statistical approaches. *Hydrological Processes*, *30*(21), 3901–3917. https://doi.org/10.1002/hyp.10913

Quinton, W. L., Gray, D. M., & Marsh, P. (2000). Subsurface drainage from hummock-covered hillslopes in the Arctic tundra. *Journal of Hydrology*, *237*(1–2), 113–125. https://doi.org/10.1016/S0022-1694(00)00304-8

Reist, J. D., Wrona, F. J., Prowse, T. D., Power, M., Dempson, J. B., Beamish, R. J., et al. (2006). General effects of climate change on arctic fishes and fish populations. *AMBIO*, *35*(7), 370–380. https://doi.org/10.1579/0044-7447(2006)35[370:GEOCCO]2.0.CO2

Runkel, R. L. (2007). Toward a transport-based analysis of nutrient spiraling and uptake in streams. *Limnology and Oceanography: Methods*, *5*(1), 50–62. https://doi.org/10.4319/lom.2007.5.50

Shuter, B. J., Finstad, A. G., Helland, I. P., Zweimüller, I., & Hölker, F. (2012). The role of winter phenology in shaping the ecology of freshwater fish and their sensitivities to climate change. *Aquatic Sciences*, *74*(4), 637–657. https://doi.org/10.1007/s00027-012-0274-3

Sinokrot, B. A., & Stefan, H. G. (1993). Stream temperature dynamics: Measurements and modeling. *Water Resources Research*, *29*(7), 2299–2312. https://doi.org/10.1029/93WR00540

Sjöberg, Y., Coon, E., Sannel, K., A. B., Pannetier, R., Harp, D., Frampton, A., et al. (2016). Thermal effects of groundwater flow through subarctic fens: A case study based on field observations and numerical modeling. *Water Resources Research*, *52*(3), 1591–1606. https://doi.org/10.1002/2015WR017571

Smith, S. L., Romanovsky, V. E., Lewkowicz, A. G., Burn, C. R., Allard, M., Clow, G. D., et al. (2010). Thermal state of permafrost in North America: a contribution to the international polar year. *Permafrost and Periglacial Processes*, *21*(2), 117–135. https://doi.org/10.1002/ppp.690

Snyder, C. D., Hitt, N. P., & Young, J. A. (2015). Accounting for groundwater in stream fish thermal habitat responses to climate change. *Ecological Applications*, *25*(5), 1397–1419. https://doi.org/10.1890/14-1354.1

Sowder&Steel, C. E. A. (2012). A note on the collection and cleaning of water temperature data. *Water*, *4*, 597–606. https://doi.org/10.3390/w4030597

Striegl, R. G., Aiken, G. R., Dornblaser, M. M., Raymond, P. A., & Wickland, K. P. (2005). A decrease in discharge-normalized DOC export by the Yukon River during summer through autumn. *Geophysical Research Letters*, *32*(21), L21413. https://doi.org/10.1029/2005GL024413

Stuefer, S. L., Arp, C. D., Kane, D. L., & Liljedahl, A. K. (2017). Recent extreme runoff observations from coastal arctic watersheds in Alaska. *Water Resources Research*, *53*, 9145–9163. https://doi.org/10.1002/2017WR020567

Toohey, R. C., Herman-Mercer, N. M., Schuster, P. F., Mutter, E. A., & Koch, J. C. (2016). Multidecadal increases in the Yukon River Basin of chemical fluxes as indicators of changing flowpaths, groundwater, and permafrost. *Geophysical Research Letters*, *43*(23), 12120–12130. https://doi.org/10.1002/2016GL070817

Turner, J., Overland, J. E., & Walsh, J. E. (2007). An Arctic and Antarctic perspective on recent climate change. *International Journal of Climatology*, *27*(3), 277–293. https://doi.org/10.1002/joc.1406

Vonk, J. E., Tank, S. E., Bowden, W. B., Laurion, I., Vincent, W. F., Alekseychik, P., et al. (2015). Reviews and syntheses: Effects of permafrost thaw on Arctic aquatic ecosystems. *Biogeosciences*, *12*(23), 7129–7167. https://doi.org/10.5194/bg-12-7129-2015

Walvoord, M. A., Voss, C. I., Ebel, B. A., & Minsley, B. J. (2019). Development of perennial thaw zones in boreal hillslopes enhances potential mobilization of permafrost carbon. *Environmental Research Letters*, *14*(1), 015003. https://doi.org/10.1088/1748-9326/aaf0cc

Walvoord, M. A., Voss, C. I., & Wellman, T. P. (2012). Influence of permafrost distribution on groundwater flow in the context of climate-driven permafrost thaw: Example from Yukon Flats Basin, Alaska, United States. *Water Resources Research*, *48*(7), W07524. https://doi.org/10.1029/2011WR011595

Yamazaki, Y., Kubota, J., Ohata, T., Vuglinsky, V., & Mizuyama, T. (2006). Seasonal changes in runoff characteristics on a permafrost watershed in the southern mountainous region of eastern Siberia. *Hydrological Processes*, *20*, 453–467. https://doi.org/10.1002/hyp.5914

Yang, D., Liu, B., & Ye, B. (2005). Stream temperature changes over Lena River Basin in Siberia. *Geophysical Research Letters*, *32*, L05401. https://doi.org/10.1029/2004GL021568

Young-Robertson, J. M., Raz-Yaseef, N., Cohen, L. R., Newman, B., Rahn, T., Sloan, V., et al. (2018). Evaporation dominates evapotranspiration on Alaska's Arctic Coastal Plain. *Arctic, Antarctic, and Alpine Research*, *50*(1), e1435931. https://doi.org/10.1080/15230430.2018.1435931

Zheng, L., Overeem, I., Wang, K., & Clow, G. D. (2019). Changing Arctic river dynamics cause localized permafrost thaw. *Journal of Geophysical Research: Earth Surface*, *124*(9), 2324–2344. https://doi.org/10.1029/2019JF005060

Zwieniecki, M. A., & Newton, M. (1999). Influence of streamside cover and stream features on temperature trends in forested streams of western Oregon. *Western Journal of Applied Forestry*, *14*(2), 106–113. https://doi.org/10.1093/wjaf/14.2.106

References From the Supporting Information

Carey, M. P., Koch, J. C., O'Donnell, J. A., & Sjöberg, Y. (2020). *Stream temperatures in the Noatak River and Kobuk River basins, Northwest Alaska, 2017–2019*. U.S. Geological Survey Data Release. https://doi.org/10.5066/P91HI62H

Jorgenson, M. T., Roth, J. E., Miller, P. F., Macander, M. J., Duffy, M. S., Wells, A. F., et al. (2009). *An ecological land survey and landcover map of the Arctic network* (Natural Resource Technical Report NPS/ARCN/NRTR 2009/270).

Koch, J. C., O'Donnell, J. A., & Carey, M. P. (2020). *Continuous records of shallow soil temperature and moisture in the Noatak River Basin, Alaska*. U.S. Geological Survey Data Release. https://doi.org/10.5066/P9048PDL

USGS EROS archive. (2016). *U.S. Geological Survey (USGS) Earth Resources Observation and Science (EROS) Center, Interferometric Synthetic Aperture Radar (IFSAR) Alaska Digital Terrain Model*. U.S Geological Survey. https://doi.org/10.5066/P9C064CO